NeuroImage 200 (2019) 159–173

Contents lists available at ScienceDirect

NeuroImage

journal homepage: www.elsevier.com/locate/neuroimage

Prospective motion correction in functional MRI using simultaneous multislice imaging and multislice-to-volume image registration

Daniel Christopher Hoinkiss [a,*], Peter Erhard [a,b], Nora-Josefin Breutigam [a], Federico von Samson-Himmelstjerna [a], Matthias Günther [a,b], David Andrew Porter [c]

[a] Fraunhofer Institute for Digital Medicine MEVIS, Bremen, Germany
[b] University of Bremen, Bremen, Germany
[c] Imaging Centre of Excellence, College of Medical, Veterinary & Life Sciences, University of Glasgow, Glasgow, Scotland, UK

ARTICLE INFO

Keywords:
Prospective motion correction
Simultaneous multislice (SMS)
Multislice-to-volume
Image registration
EPI
Functional MRI
Real-time MRI sequences
BOLD
Kalman filter

ABSTRACT

The sensitivity to subject motion is one of the major challenges in functional MRI (fMRI) studies in which a precise alignment of images from different time points is required to allow reliable quantification of brain activation throughout the scan. Especially the long measurement times and laborious fMRI tasks add to the amount of subject motion found in typical fMRI measurements, even when head restraints are used. In case of moving subjects, prospective motion correction can maintain the relationship between spatial image information and subject anatomy by constantly adapting the image slice positioning to follow the subject in real time. Image-based prospective motion correction is well-established in fMRI studies and typically computes the motion estimates based on a volume-to-volume image registration, resulting in low temporal resolution. This study combines fMRI using simultaneous multislice imaging with multislice-to-volume-based image registration to allow sub-TR motion detection with subsequent real-time adaption of the imaging system. Simultaneous multislice imaging is widely used in fMRI studies and, together with multislice-to-volume-based image registration algorithms, enables computing suitable motion states after only a single readout by registering the simultaneously excited slices to a reference volume acquired at the start of the measurement. The technique is evaluated in three human BOLD fMRI studies ($n = 1$, 5, and 1) to explore different aspects of the method. It is compared to conventional, volume-to-volume-based prospective motion correction as well as retrospective motion correction methods. Results show a strong reduction in retrospectively computed residual motion parameters of up to 50% when comparing the two prospective motion correction techniques. An analysis of temporal signal-to-noise ratio as well as brain activation results shows high consistency between the results before and after additional retrospective motion correction when using the proposed technique, indicating successful prospective motion correction. The comparison of absolute tSNR values does not show an improvement compared to using retrospective motion correction alone. However, the improved temporal resolution may provide improved tSNR in the presence of more exaggerated intra-volume motion.

1. Introduction

Functional MRI (fMRI) is commonly used to measure neural activity in the brain. This is facilitated by the BOLD (blood oxygenation level dependent) effect, which characterizes the local changes of the MR signal caused by alterations in the blood oxygenation in response to neurological tasks (Thulborn et al., 1982). To enable robust observations of brain activity, fast T_2*-weighted imaging sequences play a crucial role in measuring dynamic changes in the BOLD signal. This is why echo planar imaging (EPI, (Mansfield, 1977)) has been used for fMRI acquisitions since the first reports of functional imaging experiments (Kwong et al., 1992) (Bandettini et al., 1992). However, even with fast imaging

Abbreviations: BOLD, Blood oxygenation level dependent; CAIPIRINHA, Controlled aliasing in parallel imaging results in higher acceleration; EPI, Echo-planar imaging; fMRI, Functional MRI; FOV, Field of view; GLM, General linear model; GRAPPA, Generalized auto calibrating partial parallel acquisition; MR, Magnetic resonance; MRI, Magnetic resonance imaging; RF, Radiofrequency; SMS, Simultaneous multislice; SNR, Signal-to-noise ratio; TE, Echo time; TR, Repetition time; tSNR, Temporal signal-to-noise ratio.

* Corresponding author. Fraunhofer MEVIS, MR Physics, Am Fallturm 1, 28359, Bremen, Germany.
E-mail address: Daniel.Hoinkiss@mevis.fraunhofer.de (D.C. Hoinkiss).

https://doi.org/10.1016/j.neuroimage.2019.06.042
Received 21 December 2018; Received in revised form 14 June 2019; Accepted 18 June 2019
Available online 19 June 2019

techniques and low-resolution protocols, volume acquisition times can be long when whole-brain coverage is required. Consequently, there is the requirement for further scan acceleration to increase the temporal resolution with which the BOLD response is observed. Additionally, scan acceleration can reduce the effect of motion which occurs during the acquisition of a single image volume.

1.1. Functional MRI using simultaneous multislice imaging

Simultaneous multislice (SMS) imaging techniques acquire multiple slices simultaneously and exploit the spatial information of the coil sensitivity profiles to separate the anatomical slice information. This speeds up the acquisition by a factor equal to the slice-acceleration factor (Larkman et al., 2001). The CAIPIRINHA technique improved the image separation by introducing an in-plane image shift between the simultaneously excited slices (Breuer et al., 2005). The first SMS acquisitions in EPI sequences were presented in 2006 (Nunes et al., 2006). Since then, these techniques have been improved, for example by introducing blipped-CAIPIRINHA (Setsompop et al., 2012). This led to ultra-fast imaging which can cover the whole brain in under 300 ms when using high acceleration factors (Feinberg and Setsompop, 2013). The benefits of using simultaneous multislice imaging in functional MRI have been discussed previously (Preibisch et al., 2015) (Chen et al., 2015).

1.2. Motion effects in functional MRI

Robust data analysis in functional MRI requires, for each imaging voxel, a fixed anatomical location over the course of the measurement. This is essential to prevent artificial signal changes due to varying partial volume effects and to ensure that the BOLD response from different voxels is not mixed during data analysis. Subject motion can elevate the detection of false activation and reduce the significance of measured brain activation (Zaitsev et al., 2017). This becomes even more problematic when considering the long scan times of functional MRI studies. An additional source of motion-induced artifacts originates from spin history effects caused by inter-shot motion which yield severe banding artifacts in the images. Motion in fMRI studies can be categorized by different sources. During the long measurements, human subjects tend to slowly move in a specific direction, for example by sinking into the padding used for comfort and head restraint, leading to long-term, rigid-body motion. Fast motion events coming from coughing and swallowing or when measuring uncooperative subjects may happen in addition and require high temporal resolution of motion correction procedures. These noticeable effects might even be increased when measuring with a head restraint (Bettinardi et al., 1991; Edward et al., 2000). A third category is periodic motion as is caused by respiration or cardiac pulsation. Respiratory motion effects are further increased by susceptibility changes in the head region caused by movements of the chest and become more visible when measuring with high temporal resolution, as in functional MRI using simultaneous multislice imaging (Cheng and Puce, 2014).

1.3. Motion correction in functional MRI

Retrospective motion correction is the most commonly used method when handling functional MRI data. Data analysis software packages, e.g. FSL (Jenkinson et al., 2002), AFNI (Cox, 1996) or SPM (Friston et al., 2007), typically include algorithms for retrospective motion correction, treating the motion as a pure rigid-body process and correcting on a volume-to-volume basis. Detected motion parameters can optionally be used as confounding model parameters in the general linear model (GLM) to reduce motion-induced effects in the fMRI statistics (Friston et al., 2007). Since these algorithms mostly work with a volume-to-volume-based image registration, intra-volume motion effects are not considered in the correction process and correction of fast motion events is difficult. Simultaneous multislice fMRI mitigates this by reducing the repetition time between successive image volumes. But, in most cases, this is still too slow to reconstruct the correct course of, for example, respiratory motion. To solve this challenge, there are recent developments of post-processing algorithms for performing slice-wise motion correction to improve the fMRI analysis, such as SLOMOCO (Beall and Lowe, 2014). A large problem of retrospective motion correction is that data which were lost during image acquisition cannot be restored later, for example when the subject moves out of the field of view during the scan such that information about some anatomical regions of interest is not available throughout the whole measurement. Additionally, subject motion can cause MR-signal loss caused by the aforementioned spin history effects that introduce spatial variation in image contrast and cannot be repaired by retrospective motion correction techniques without Bloch simulations (Thesen et al., 2000). All retrospective motion correction techniques require data interpolation when transforming the image data to account for the subject motion. This procedure can degrade spatial resolution and previous work (Thesen et al., 2000) has suggested that this is less of an issue when prospective motion correction is used to reduce the level of residual motion that has to be corrected retrospectively.

Prospective motion correction, first introduced in Haacke and Patrick (1986), helps to maintain a fixed relationship between subject and imaging geometry. Disadvantages associated with retrospective motion correction, such as spin history effects, interpolation artifacts and the inability to recover lost image data, can be solved in principle by prospective motion correction algorithms, but in practice these can also destabilize the imaging system when the accuracy of motion correction updates is not sufficient (Zaitsev et al., 2017). Most fMRI studies using prospective motion correction without external hardware rely on volume-to-volume-based motion detection (Thesen et al., 2000). The big downside of this approach is its low temporal resolution and missing intra-volume motion correction. Temporal resolution can be improved by accelerating the image acquisition with SMS imaging techniques. However, the temporal resolution might not be high enough to cover fast motion events. Image-based prospective motion correction needs some computation time for image reconstruction and motion detection. This requires a short inter-volume delay or, alternatively, skipping a volume before applying motion updates with the disadvantage that the temporal resolution of the correction procedure is reduced (Zaitsev et al., 2017). In Teruel et al. (2018), the established PROMO technique (White et al., 2010) was transferred to simultaneous multislice fMRI to retrospectively estimate motion with sub-TR resolution and might be applicable for prospective motion correction in the future. Another way to achieve a significant improvement in the temporal resolution of prospective motion correction is the use of external hardware for motion detection as for example in camera-based prospective motion correction (Zaitsev et al., 2006; Aksoy et al., 2011; Huang et al., 2018). These methods have high accuracy and update rates, but need additional, potentially expensive hardware and a preparation step prior to the scan. They rely on external markers to be tracked by the cameras, which can be uncomfortable to the subject. Furthermore, optical systems only detect the motion of the scalp which might not precisely represent the actual motion of the brain. On the other hand, image registration algorithms as used in image-based prospective motion correction may also use information from the neck which might not follow the rigid-body motion of the head. Registration accuracy can also be affected by image distortions that are particularly present in EPI images of lower slices of the brain and vary with subject motion (Andersson et al., 2018).

1.4. Prospective motion correction using multislice-to-volume image registration

This work transfers the idea of multislice-to-volume image registration for prospective motion correction, introduced in Hoinkiss and Porter (2017), to simultaneous multislice fMRI. The previous work showed that registering a subset of slices to a full image volume allows robust

prospective motion correction. The fastest way to acquire this subset of slices is given by simultaneous multislice imaging, such that only a single radiofrequency (RF) excitation is necessary to acquire the required image slices for motion detection. This can significantly speed up the temporal resolution of motion parameter updates in comparison to volume-to-volume-based approaches and enables the correction of fast motion events, including those happening during the acquisition of a single imaging volume. Functional MRI based on single-shot EPI is well suited to this correction method because a self-navigated approach can be used without the additional navigators used in the previous study. Furthermore, the SMS technique is already widely used in functional MRI studies, so the correction method can be implemented without any impact on the scanning protocols used. The technique is evaluated using fMRI paradigms which examine the brain activation as a result of repeated visual and motoric tasks using imaging protocols with slice-acceleration factors of three and four. Some of this work has previously been reported in abstract form (Hoinkiss et al., 2018).

2. Material and methods

Fig. 1 shows an overview of the image acquisition and multislice-to-volume-based prospective motion correction of a simultaneous multislice fMRI acquisition. It includes the acquisition of single-band SMS auto-calibration data (1) and the generation of an SMS reference volume for motion correction (2) at the start of the measurement. The imaging scans are then acquired using simultaneous multislice EPI measurements where simultaneously acquired slices are separated in real time (3). The separated imaging slices are used as input for a multislice-to-volume image registration (4) and the motion parameter updates are sent back to the imaging system in real time (6). This step uses the motion estimates to derive a linear quaternion-based transformation of the imaging slice to compensate for the detected motion. Scanner hardware is adapted by altering the logical gradient orientations as well as rf pulse frequencies and phases (Maclaren et al., 2013). A Kalman filter is used to smooth the motion correction updates during the scan to give reliable motion parameter estimates (5). It can also be skipped when filtering of the motion parameters is not desired. These steps are described in more detail in the following sections.

2.1. Method overview

The first step of the imaging process involves acquiring the single-band SMS auto-calibration data (see Fig. 1, step 1). The auto-calibration slices experience the same image shift as the subsequent imaging scans and are used to calculate the required GRAPPA weights which connect the spatial information of the image volume to the coil sensitivity profiles (Setsompop et al., 2012). An adapted slice-GRAPPA algorithm, developed by Cauley et al. (2014), called split slice-GRAPPA, is used, which reduces inter-slice leakage artifacts. The GRAPPA-weights calculation is usually time consuming. However, by parallelizing the computations on all scanner processor threads, this time can be highly reduced, making it suitable for real-time applications. Subsequent SMS imaging scans are separated in real time using the previously calculated GRAPPA weights. The first reconstructed SMS volume is used as a reference volume for the prospective motion correction (see Fig. 1, step 2). The next SMS imaging slices are disentangled (see Fig. 1, step 3) and used as input for a multislice-to-volume image registration to the reference volume (see Fig. 1, step 4). This image registration is based on the Mattes' mutual information metric (Mattes et al., 2001; Mattes et al., 2003) and a 3D rigid versor transform and optimization (ITK 3.8.0 (Yoo et al., 2002), open source). Both the slice separation as well as the image registration are parallelized on the scanner processor threads to reduce computation times. The estimated motion parameters are sent back to the imaging system, such that subsequent SMS imaging scans are acquired using the updated slice information (see Fig. 1, step 6). Using this feedback cycle, continuous prospective motion correction is performed with the objective of maintaining a fixed relationship between subject and imaging plane.

2.2. Kalman filtering to smooth motion parameter estimates

Multislice-to-volume image registration uses much less image data to detect the motion parameters than conventional volume-to-volume-based image registration algorithms. In the case of outliers in the motion detection estimates or instability of the system, a Kalman filter can reduce noise and registration errors originating from the motion detection procedure (see Fig. 1, step 5). In the prospective motion correction, the state vector of the Kalman filter does not describe the absolute

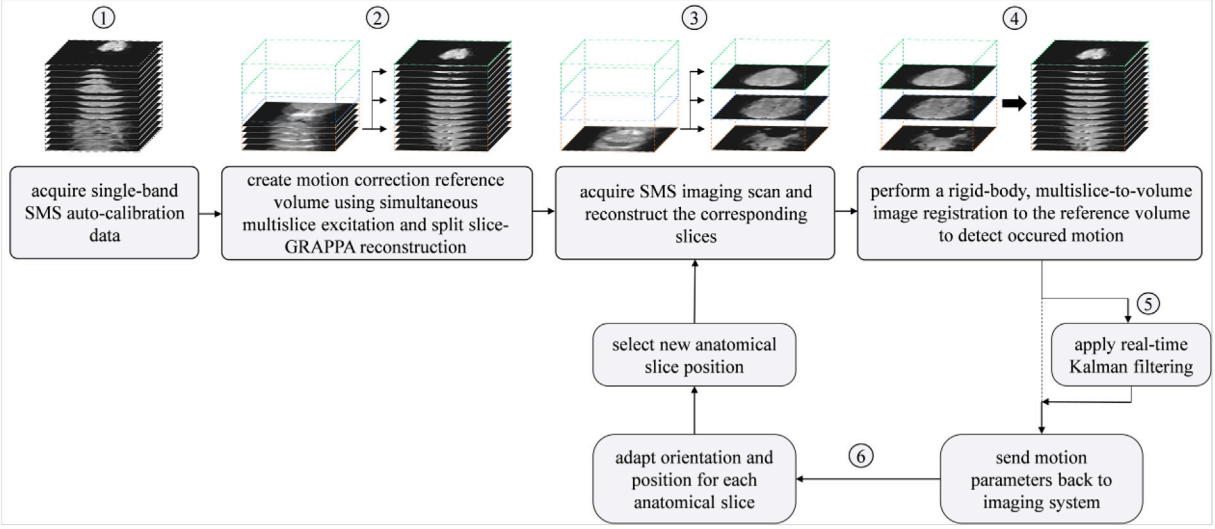

Fig. 1. Overview of the proposed prospective motion correction technique using multislice-to-volume image registration in simultaneous multislice fMRI for a slice-acceleration factor of 3. The technique includes the acquisition of a single-band SMS auto-calibration volume (1), the acquisition of an SMS reference volume for the prospective motion correction (2), the SMS imaging scans (3) which are used as input for a multislice-to-volume image registration (4) and the real-time feedback to the sequence to adapt the imaging system according to the detected motion (6). A real-time Kalman filter can be added for parameter smoothing in the case of instability of system (5).

distance between subject and imaging geometry, since this would introduce overshooting of the filter, but the time course of accumulated motion detection estimates. This makes it possible to follow the true estimated subject motion during the measurement. It is implemented as single one-dimensional Kalman filters for each degree of freedom of the rigid-body motion detection, where each degree of freedom is calculated on a different scanner processor thread. This simplifies the filtering process to a one dimensional Kalman filter in which we consider subject position and velocity in the prediction model, resulting in a state vector $x = (s, \dot{s})$ which is initialized as $x_0 = (0, 0)$ at the start of the measurement. The current prediction is used at each time point to adapt the estimated motion parameter to the underlying system, weighted by the calculated Kalman gain which depends on the expected measurement and process noise. More details on Kalman filtering can be found in Kalman (1960). The drawback of this procedure is the obvious delay in reacting to fast subject motion to which the filter model does not adapt instantly.

Kalman filtering has been used previously in the prospective motion correction of MRI acquisitions, for example for improving the results of camera-based methods (Maclaren et al., 2009) or for image-based tracking (White et al., 2010).

3. Experiments

Experiments were performed on a 3 T MR system with a 20-channel head coil (MAGNETOM Skyra, software version Syngo MR D13A, Siemens Healthcare, Erlangen, Germany). All subjects provided written informed consent prior to scanning and the study was approved by the local ethics committee.

To evaluate the suggested motion correction method, a dedicated simultaneous multislice fMRI sequence with a multi-threaded implementation of the split slice-GRAPPA image reconstruction algorithm was developed and modularly combined with three different prospective motion correction scenarios:

- volume-to-volume-based prospective motion correction,
- multislice-to-volume-based prospective motion correction and
- no prospective motion correction.

The sequence used fat saturation pulses prior to slice excitation and no in-plane GRAPPA was performed. The pulse sequence, split slice-GRAPPA reconstruction, image registration and real-time correction algorithms were implemented using the manufacturer's proprietary pulse-sequence and image-reconstruction development frameworks together with the ITK 3.8.0 image processing library, which was used for computing the multi-threaded multislice-to-volume image registration. The volume-to-volume-based prospective motion correction was added using the vendor-specific modules for prospective motion correction in functional MRI (Thesen et al., 2000).

The flip angle of the RF excitation was adapted to the repetition time by calculating the Ernst angle with an average T_1 in gray matter of 1331 ms at 3 T as reported in Wansapura et al. (1999). B_0-field correction (Thesen et al., 2003; Benner et al., 2006) was used when measuring without prospective motion correction. In the measurements with applied prospective motion correction, the B_0-field drifts were corrected by the motion correction procedure, meaning that the associated subject drift in phase-encoding direction was interpreted as motion and corrected by the motion correction procedure. This way, the dynamic B_0-field drift and motion correction procedures do not interfere. However, because the system operation frequency was not adapted, the B_0-field drift could affect the fat saturation during long measurements. A waiting time was introduced into the pulse sequence immediately after acquiring the SMS auto-calibration data for calculation of the GRAPPA weights.

Both prospective motion correction algorithms were implemented such that each EPI slice position was corrected using the most recently calculated motion update available.

In all functional measurements, the same fMRI paradigm was used. The visual cortex was stimulated by displaying an inverting checkerboard. Simultaneously, the volunteers performed a button-pressing task with both hands to stimulate the motor cortex. The order of the required button presses was communicated prior to each activation phase and changed throughout and between the scans. Activation phases of 22 s alternated with resting phases of 22 s in 5 min long measurements. Prior to each image volume acquisition, a trigger pulse was sent from the MRI scanner to the fMRI task hardware to synchronize pulse sequence and fMRI paradigm.

3.1. Technical evaluation on the accuracy of multislice-to-volume image registration

A first experiment was performed in silico to evaluate the accuracy and limitations of the multislice-to-volume image registration by a comparison to its volume-to-volume counterpart. The experiment was performed using data from the same imaging sequence as described in the experiments below. Image registration was performed for each time point and all possible slice positions that could be excited simultaneously in an SMS EPI measurement. Registration accuracy was evaluated by a comparison to the results of volume-to-volume image registration when using different numbers of slices for the registration process. For both image registration methods, the exact same image registration setup was used (utilizing mutual information as used by the multislice-to-volume registration in all subsequent experiments).

3.2. Single-subject study with and without voluntary head motion

An experiment with a single subject (male; aged 28) was performed in vivo to examine the effect of the different prospective motion correction scenarios on scans with intentional head movement. The subject was told to randomly move his head in the head coil. No head restraint was used throughout the measurements, but the radius of the movements was restricted by the earmuffs and the head coil. All three implemented variants of the simultaneous multislice fMRI sequence were measured both with and without voluntary subject motion and the scan order was randomized throughout the study. Data were acquired using the dedicated T_2*-weighted gradient-echo SMS-EPI sequence, described previously. 42 slices were scanned using TE/TR values of 30 ms/1100 ms, $(3\ \text{mm})^3$ isotropic voxel size, no slice gap, a matrix size of 64 by 64, a flip angle of 64°, 660 μs echo spacing, and a (3 × 3) split slice-GRAPPA kernel size. All measurements used a slice-acceleration factor of three and the measurement time was 5 min. In this initial experiment, no real-time Kalman filtering was used. Residual motion parameters of the acquired image time series were calculated using retrospective motion correction algorithms in SPM12 (Friston et al., 2007) and the results were compared between the different sequence variants.

3.3. Five-subject functional MRI study without voluntary head motion

A second experiment included five subjects (3 female, 2 male; aged between 22 and 33) and was performed in vivo without intentional head movements. However, no head restraint was used, such that the possibility of involuntary head motion was increased. Additionally, there was an increased chance of motion related to performing the paradigm tasks during the fMRI procedure. Each subject was scanned six times with 5 min long sequence protocols, involving all three sequence variants (no prospective motion correction, volume-to-volume-based prospective motion correction and multislice-to-volume-based prospective motion correction) for slice-acceleration factors of three and four. Measurement order was again randomized to reduce experimental bias. Both imaging protocols acquired data from 36 slices with 3 mm isotropic voxel size, no slice gap, a matrix size of 64 by 64, an echo time of 30 ms, 660 μs echo spacing, and a (3 × 3) split slice-GRAPPA kernel size. Based on the Ernst angle, the flip angle was chosen to be 59° at a repetition time of 890 ms

for the protocol with a slice-acceleration factor of three and 53° at a repetition time of 670 ms for the protocol with a factor of four. All other scan protocol parameters were equal to the previous experiment. The real-time Kalman filter was used in the multislice-to-volume-corrected sequences to add stability to the prospective motion correction system. Data were analyzed by calculating the residual motion parameters using SPM12 as well as the mean voxel displacement, which combines the six rigid-body motion parameters by calculating the displacement for each anatomically located voxel, relative to a reference image, and averaging it over all voxels of the current imaging volume. In addition, the voxel-by-voxel temporal signal-to-noise ratio (tSNR), which compares the time-course mean of a voxel to its standard deviation, was calculated and analyzed qualitatively using color-coded imaging data and quantitatively by averaging these data over all image voxels. SPM12 was also used to determine the measured brain-activation maps from which the mean of the top 10% of t-values was extracted to compare brain activity between measurements. This analysis was performed both with and without additional retrospective motion correction. The post processing included smoothing with a [6 6 6] full width at half maximum Gaussian kernel, high-pass filtering and, in the case of retrospective motion correction, motion detection, image realignment and co-registration to a standard space. In the latter case, all six motion parameters were added as confounds in the GLM design matrix.

3.4. Functional MRI with repeated breathhold events

The last experiment was performed on a single subject (male; aged 60) to evaluate the influence of respiratory motion on slice-accelerated functional MRI and to see if the multislice-to-volume motion detection can successfully reconstruct the underlying respiratory motion events. The volunteer was told to alternate between phases of normal respiration and breathhold, instructed by a visual cue. The same imaging protocol as in the five-subject experiment was used for a slice-acceleration factor of four and the subject motion was reconstructed by accumulating the Kalman-filtered motion correction events. Additionally, a respiratory cushion was used to monitor the true respiration of the volunteer. The respiratory cushion was provided by the scanner vendor.

4. Results

4.1. Technical evaluation on the accuracy of multislice-to-volume image registration

Fig. 2 shows the results of the first experiment on the accuracy of multislice-to-volume image registration. The results for two different motion parameters are plotted over the time of the 5 min long measurement with noticeable subject motion. The red curve shows the volume-to-volume image registration results for each time point with respect to a reference image. The multislice-to-volume image registration results for all individual slice positions are displayed as error bands, showing the standard deviation around the mean value for each time point. The calculation was performed for multislice-to-volume image registration using one (blue), two (orange), three (green), four (red) and five (purple) slices. It shows a wide error band when only using one slice. This error is reduced by adding a second slice to the image registration. However, the standard deviation is further reduced when using three slices or more as seen by the green, red and purple error bands. These are centered around the volume-to-volume reference and the respective errors are similar. This led to the decision to use slice-acceleration factors of three and four in the subsequent experiments as a compromise between image quality and robust image registration.

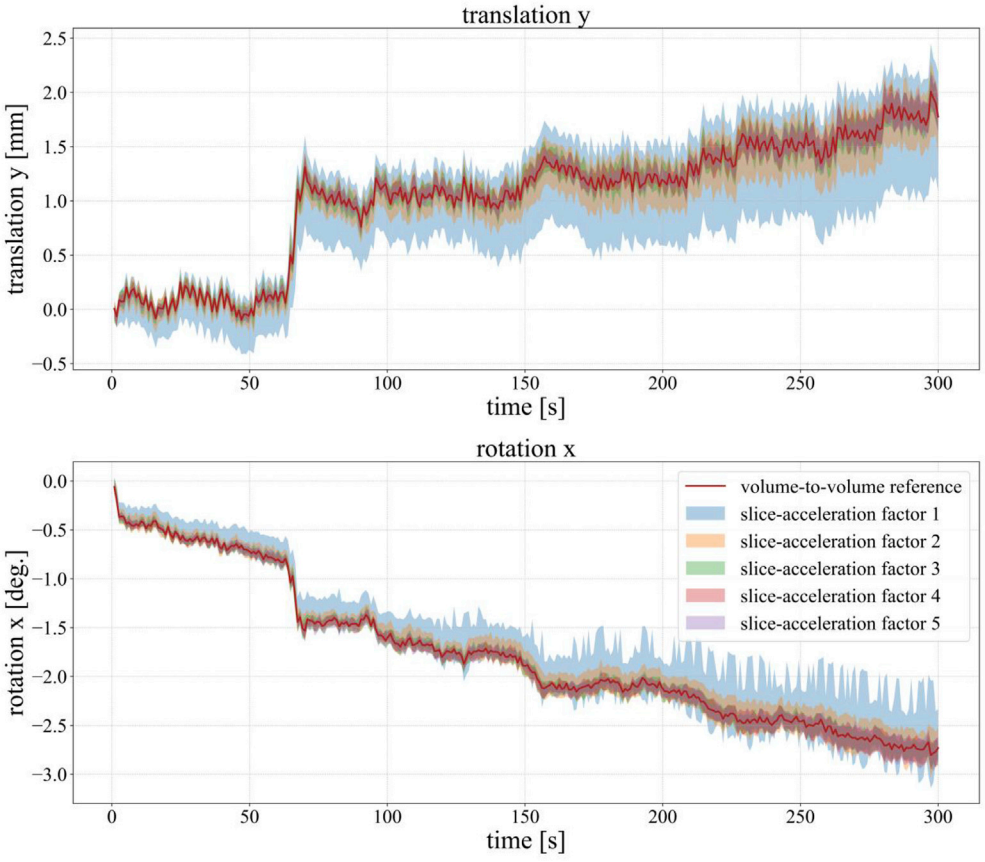

Fig. 2. Image registration results from measurement data acquired in vivo without prospective motion correction. It shows significant subject motion during a 5 min long measurement, displayed for translational motion in y-direction (top) and rotational motion in x-direction (bottom). The red curve shows the image registration results when performing volume-to-volume image registration as reference. For each time point, the multislice-to-volume image registration results are plotted as the standard deviation around the mean value of all possible slice positions, displaying the accuracy of the method when using different slice positions. This is depicted for image registration using one (blue), two (orange), three (green), four (red) and five (purple) slices for the image registration.

4.2. Timing and calculation times of the multislice-to-volume-based prospective motion correction

Analyzing the processing times of the different tasks when acquiring images with multislice-to-volume-based prospective motion correction shows a typical time to separate the simultaneously excited slices of 40–50 ms and to calculate the multislice-to-volume image registration of 70–100 ms. The slice position and orientation of the sequence was always updated prior to the slice excitation by checking the latest calculated motion state. This enabled a temporal resolution of motion correction updates for the multislice-to-volume-based prospective motion correction which was below an upper limit of 300 ms in all experiments. This includes also the conventional image reconstruction steps as well as the time between finishing the image registration and applying the motion update at the start of the next EPI slice acquisition. However, compared to volume-to-volume-based prospective motion correction using the same SMS EPI scan protocol, which required a skip of one TR to compute the motion detection and update the FOV geometry in our experimental setup, the multislice-to-volume-based approach increases the temporal resolution of motion correction updates by factors of ~6 and ~4.5 when scanning with slice-acceleration factors of three and four, respectively.

4.3. Single-subject study with and without voluntary head motion

The increase in temporal resolution results in faster adaption to subject head motion, as depicted in Fig. 3. This figure shows the residual motion parameters over the time course of the first measurements acquired in vivo (slice-acceleration factor three) with voluntary head motion, retrospectively calculated by SPM12. This initial experiment did not use the Kalman filter to stabilize the motion parameters. The left column shows the extent of motion, performed by the subject, without any prospective motion correction. Volume-to-volume-based prospective motion correction (mid column) did not provide stable motion parameter estimates and shows a high level of residual subject motion. Additionally, high-frequency motion components further destabilize the motion estimates. The higher temporal resolution of multislice-to-volume-based prospective motion correction (right column), however, was able to provide data with low residual motion of ±0.5 mm/± 0.5° in all six degrees of freedom. As with all data in this section, the underlying motion was not strictly controlled hence it cannot be assumed to be identical between the different measurements.

The results of the same experiment without intentional head motion in Fig. 4 still reveal noticeable subject motion, as seen in the measurements without prospective motion correction (left column). These motion events, however, consist of fewer periods of fast motion, but show typical long-term subject motion. The volume-to-volume-based prospective motion correction (mid column) shows low residual motion parameter estimates which are evenly distributed about $y = 0$. The residual motion parameters when using the multislice-to-volume-based prospective motion correction (right column) are dominated by single outliers which distract the motion correction at different time points as seen, for example, in the curves of translation in x-direction and rotation in y-direction at the 150 s mark, before tending back to the x-axis. This might be caused by false registrations of the multislice-to-volume image registration given the low amount of image information. In all the following measurements described below, this effect was prevented by applying the Kalman filtering of the feedback data to stabilize the motion estimates during the prospective motion correction procedure.

4.4. Five-subject functional MRI study without voluntary head motion

With the addition of the Kalman filter to the prospective motion correction, the residual motion parameters of multislice-to-volume-based prospective motion correction remain stable, as seen by the retrospectively detected residual motion parameters (SPM12) in Fig. 5. The diagrams display residual motion parameters from a single measurement without intentional head motion, using a slice-acceleration factor of three. Despite the visible subject motion when scanning without prospective motion correction (left column), the multislice-to-volume-based approach (right column) was able to produce image data with considerably low residual motion without noticeable outliers. The volume-to-volume-based prospective motion correction (mid column) shows

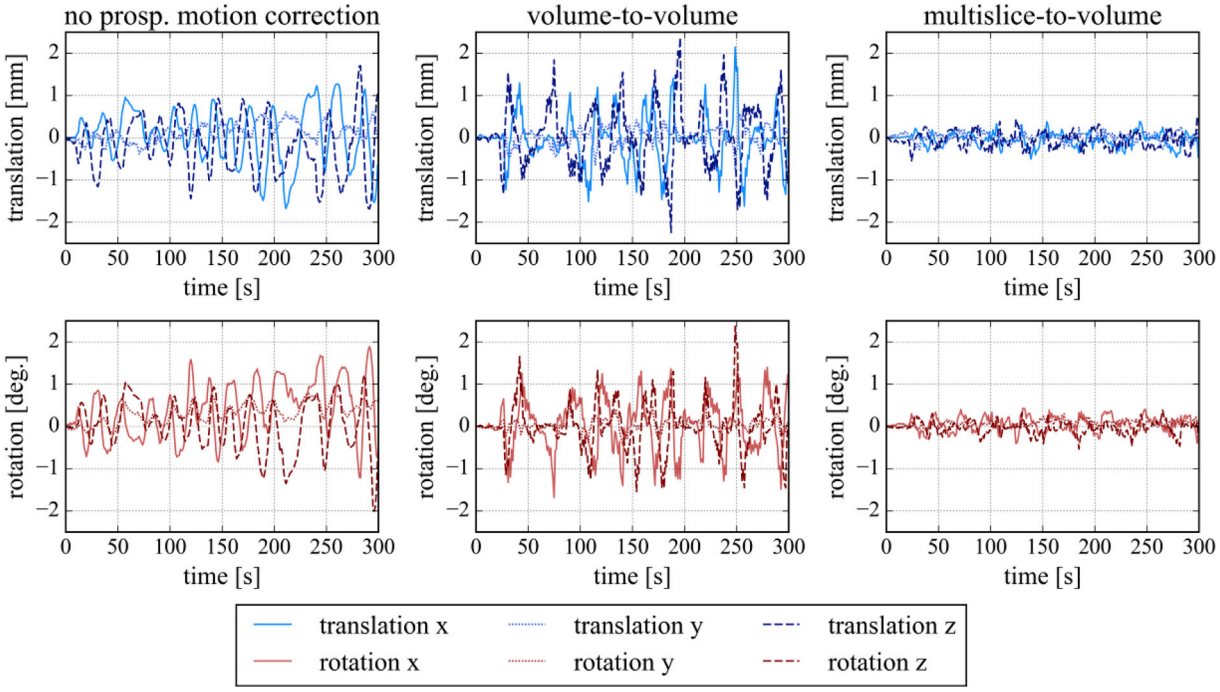

Fig. 3. Motion parameter estimates derived by SPM12 post processing for measurements acquired while performing an fMRI task and random, intentional head movements. The curves show the residual motion without prospective motion correction (left column), after volume-to-volume-based prospective motion correction (mid column), and after multislice-to-volume-based prospective motion correction (right column).

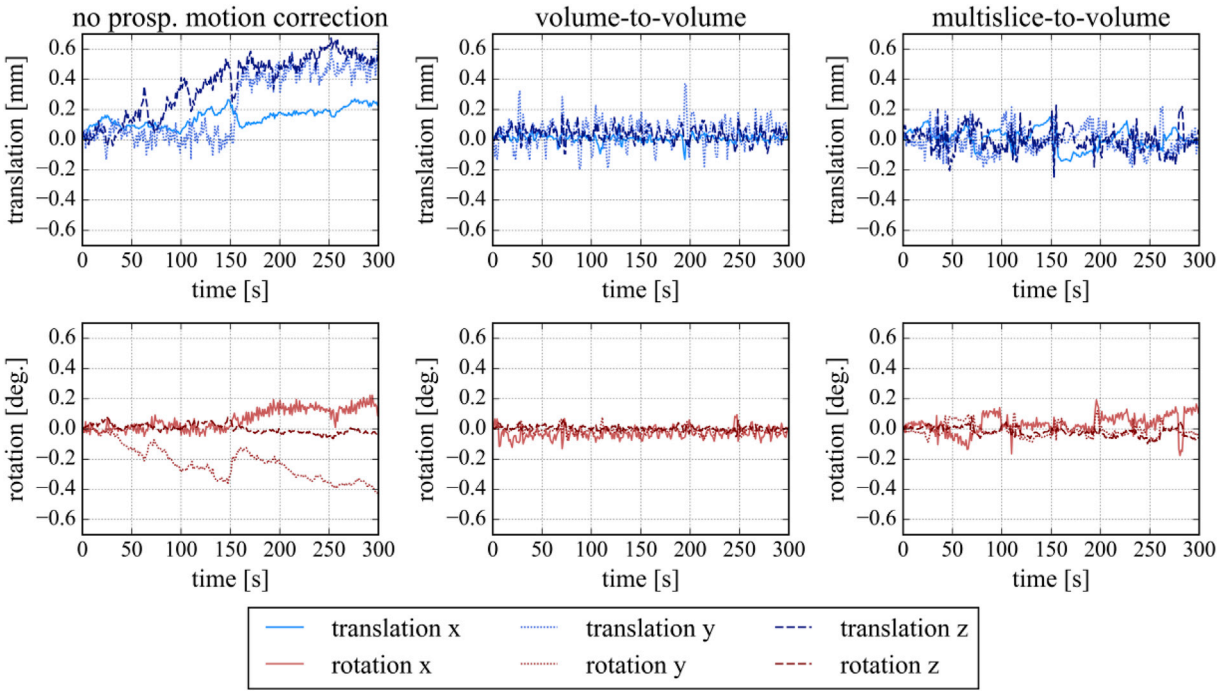

Fig. 4. Motion parameter estimates derived by SPM12 post processing for measurements acquired without prospective motion correction (left column), after volume-to-volume-based prospective motion correction (mid column), and after multislice-to-volume-based prospective motion correction (right column). The volunteer performed a typical fMRI task during the measurement without intentional head movements.

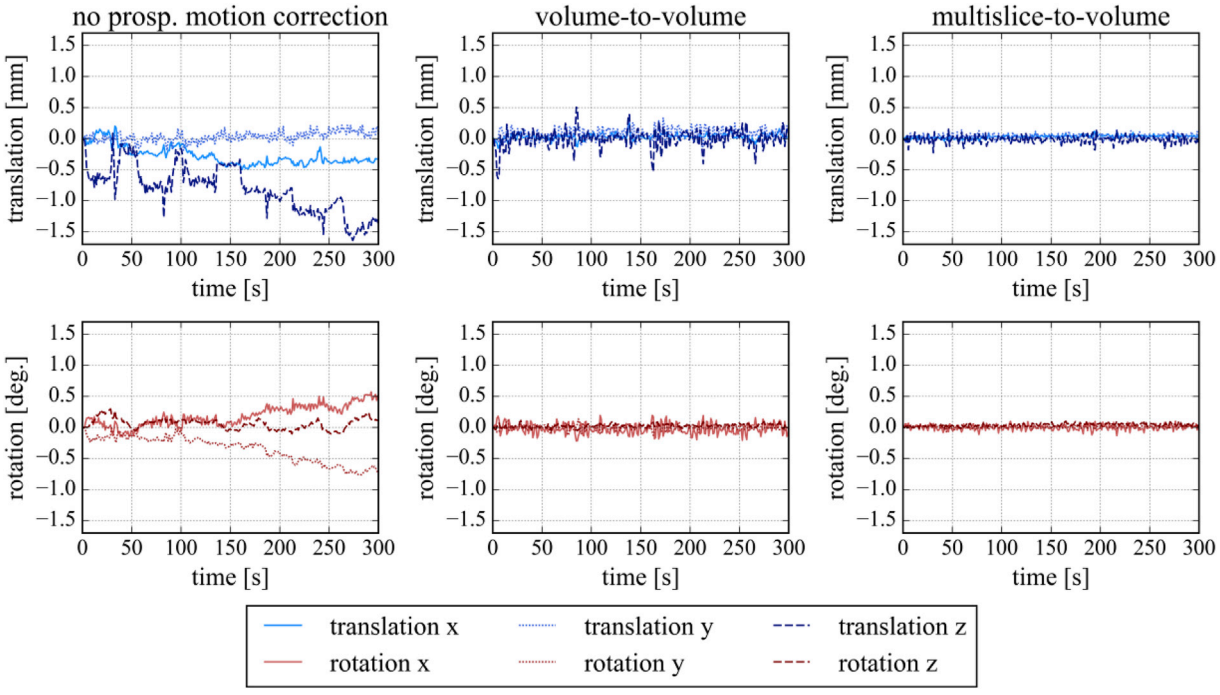

Fig. 5. Motion parameter estimates derived by SPM12 post processing for measurements acquired without prospective motion correction (left column), after volume-to-volume-based prospective motion correction (mid column), and after multislice-to-volume-based prospective motion correction (right column). The multislice-to-volume-based prospective motion correction used the Kalman filtering of motion correction updates during the scan to account for fluctuations in the registration process.

noticeable fluctuation in residual motion parameters. This can be quantified by the mean standard deviation over the six motion components which is 0.075 for the volume-to-volume-based approach and 0.035 for the multislice-to-volume-based approach.

Fig. 6 depicts the absolute mean residual motion parameters of all subjects and measurements of the five-subject experiment. All measurements were performed without intentional head motion and without head restraint. The residual motion parameters were estimated by calculating the mean and standard deviation of the absolute motion values estimated by SPM12 retrospective motion detection. The

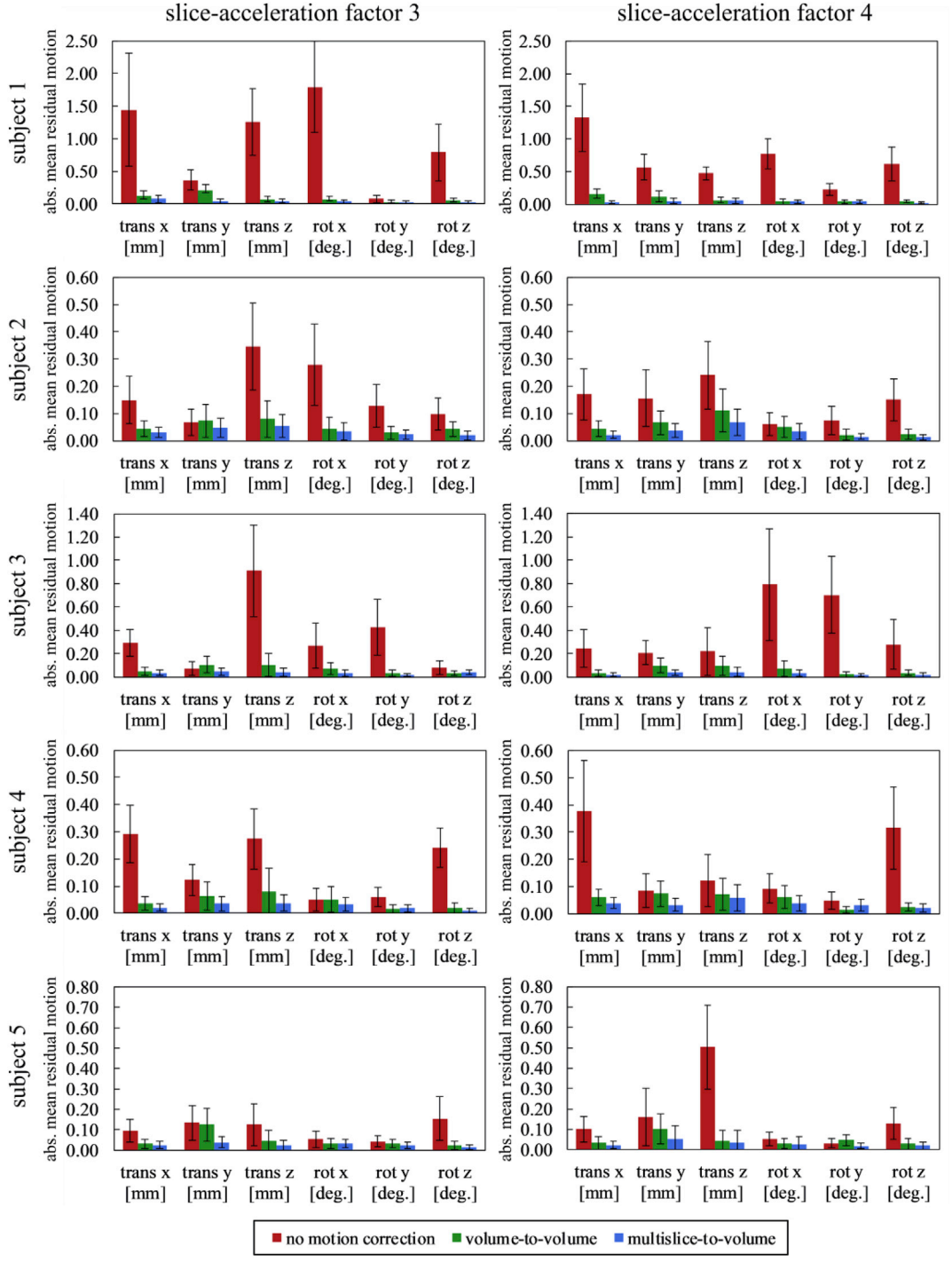

Fig. 6. Absolute mean and standard deviation of residual motion parameters across the five subjects and slice-acceleration factors of three and four. The red bars show the absolute mean residual motion parameters when measuring without prospective motion correction, the green bars depict the results with volume-to-volume-based prospective motion correction and the blue bars, which show the least amount of absolute mean residual motion, are the results of measurements which were prospectively corrected using the multislice-to-volume-based technique. The motion estimates were calculated based on the results of SPM12 retrospective motion detection.

diagrams show the results for each subject and slice-acceleration factor. They display the mean residual motion parameters for the six degrees of freedom (three for translation, three for rotation) and for all prospective motion correction scenarios: no prospective motion correction (red), volume-to-volume-based prospective motion correction (green) and multislice-to-volume-based prospective motion correction (blue). Each subject showed a different amount of involuntary motion in the measurements, indicated by the red bars. Both prospective motion correction techniques were able to reduce the amount of absolute mean residual subject motion to below 0.1 mm or 0.1° in all cases. Comparison of both prospective motion correction strategies shows that the multislice-to-volume-based prospective motion correction provides the lowest mean value of residual motion parameters. However, the error bars, which depict the standard deviation of residual motion parameters, suggest that this is not a significant effect in all cases.

The results of the six rigid-body motion parameters can be combined

by calculating the mean voxel displacements, as shown in Fig. 7. Both prospective motion correction methods are compared for all five subjects and both slice-acceleration factors. Again, the results of the volume-to-volume-based prospective motion correction are displayed in green and those of the multislice-to-volume-based prospective motion correction in blue. The diagrams show a strong reduction in mean voxel displacements for the multislice-to-volume-based approach compared to the volume-to-volume-based method, showing improvements in mean voxel displacement of 50.9% and 46.6% for the slice-acceleration factors three and four, respectively.

Fig. 8 shows the tSNR maps of one of the five subjects with a slice-acceleration factor of three for all three prospective motion correction scenarios. The tSNR data are shown both without (left) and with (right) retrospective motion detection and image alignment, calculated by SPM12. The tSNR maps suggest that, without any prospective motion correction (see Fig. 8a), tSNR is very low when compared to the resulting images of measurements with applied prospective motion correction (see Fig. 8b and c). Between the two different prospective motion correction techniques, the multislice-to-volume approach shows slightly higher tSNR values, particularly in the upper image slices (see Fig. 8c). With additional retrospective motion correction (see Fig. 8d–f), these differences are considerably reduced showing that retrospective motion correction is able to provide similar results in all three cases despite the severe differences in tSNR before applying retrospective motion correction. However, the top and bottom slices of measurements with volume-to-volume-based prospective motion correction (see Fig. 8e) or no prospective motion correction (see Fig. 8d) are cut off. This is an effect of image transformations that are needed to align the time-course images retrospectively when a high amount of residual motion is present.

The bar plots, displayed in Fig. 9, show the tSNR results of all five subjects. The temporal SNR values are calculated on foreground-masked image volumes (Huang and Wang, 1995) and plotted for each measurement. The foreground masking algorithm excluded all background noise voxels from the statistics to calculate a global tSNR value on the subject anatomy. Temporal SNR values are displayed both for slice-acceleration factors of three (top row) and four (bottom row) as well as without (red, green, blue) and with (light red, light green, light blue) retrospective motion correction using SPM12. The figure shows that retrospective motion correction improves the tSNR in all subjects when measuring without prospective motion correction. Results from measurements with prospective motion correction, however, are consistent when comparing tSNR values before and after additional retrospective motion correction. An analysis of absolute values of all three prospective motion correction scenarios with additional retrospective motion correction shows no significant advantage of one of the methods. Retrospective motion correction was, in all cases, able to provide similar temporal SNR values. The results also indicate that the tSNR is reduced by a general image quality degradation at higher slice-acceleration factors.

The following part of this section discusses the fMRI brain activation results. Fig. 10 shows the brain activation map and the BOLD response in the area of highest activation of the visual cortex for a measurement acquired with prospective motion correction utilizing multislice-to-volume motion correction and without additional retrospective motion correction. The curves show the fitted model as well as the residual signal variance in the voxel which is not explained by the model.

Results of the brain activation analysis in terms of the mean of the top 10% of t-values for both slice-acceleration factors are shown in Fig. 11. The data show strong variation in measured brain activation between measurements and subjects. The figure highlights the changes in the t-value metric when using additional retrospective motion detection and image realignment in measurements with no prospective motion correction (red), volume-to-volume-based prospective motion correction (green), and multislice-to-volume-based prospective motion correction (blue). Results of measurements with multislice-to-volume-based prospective motion correction show high consistency between the t-value statistics before (blue) and after (light blue) additional retrospective motion correction. When using the volume-to-volume-based prospective motion correction, t-values are increased by the retrospective image realignment. Measurements without prospective motion correction show a different effect. Here, retrospective motion correction strongly reduces the brain activation in the data. Observing the motion detection estimates of these data suggests that this is related to false activation due to task-related motion performed by the subjects (data not shown).

Regarding absolute brain activation results, a comparison of the measurements with additional retrospective motion correction shows over 50% higher t-values on average when using one of the two prospective motion correction techniques; 53.46% ± 56.70% for volume-to-volume and 56.70% ± 40.45% for multislice-to-volume-based prospective motion correction. Comparing the two prospective motion correction methods to each other shows comparable results regarding absolute brain activation.

4.5. Functional MRI with repeated breathhold events

The bottom graph of Fig. 12 depicts data from the respiratory cushion during MRI scanning. It shows the phases of normal respiration and breathhold throughout the measurement. The frequency of respiration during this experiment was ~0.34 Hz which would require a sampling

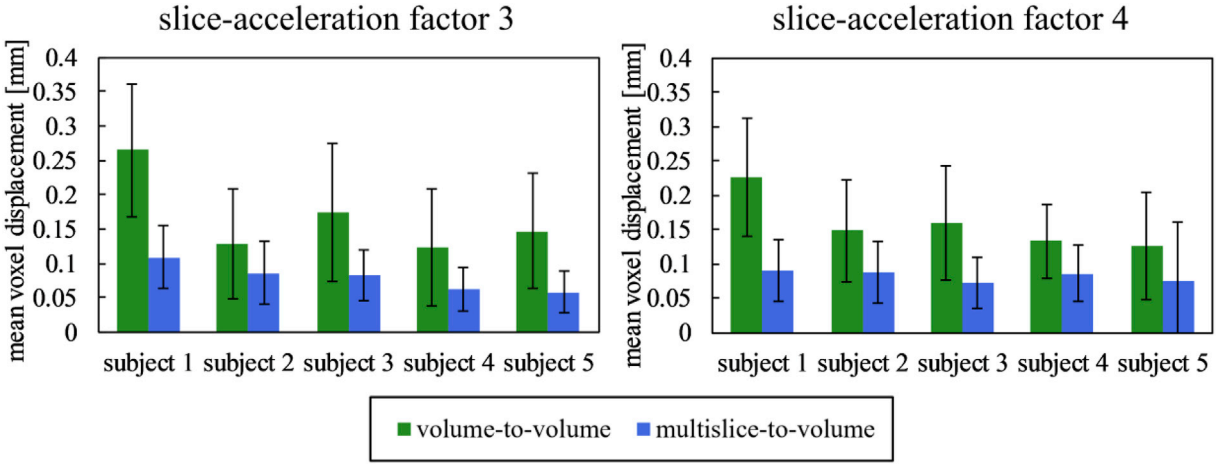

Fig. 7. Comparison of mean voxel displacement and standard deviation for measurements with volume-to-volume-based (green) and multislice-to-volume-based (blue) prospective motion correction across all five subjects and for slice-acceleration factors of three and four. The mean voxel displacements were calculated based on the results of SPM12 retrospective motion detection.

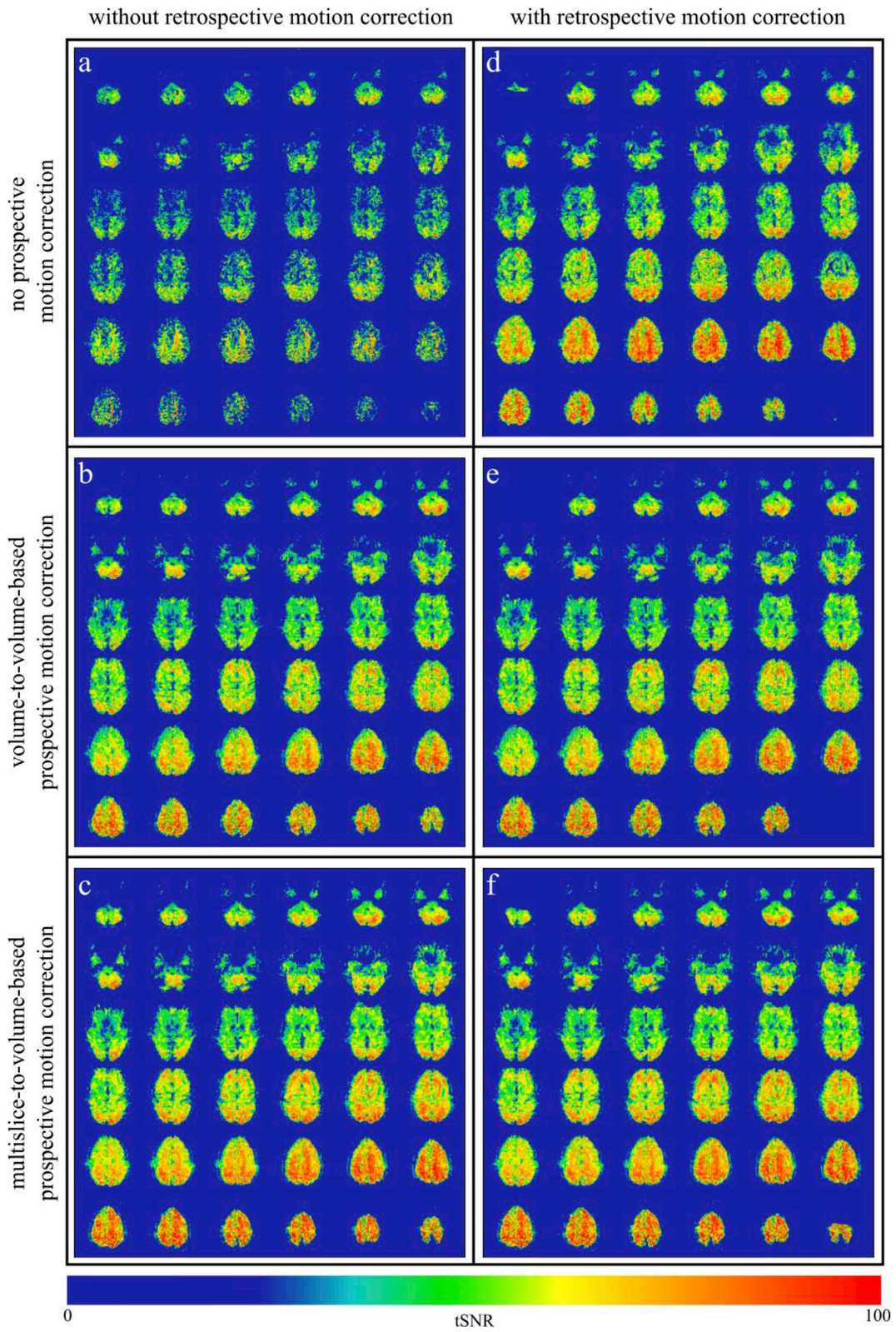

Fig. 8. Temporal SNR maps of a single subject from measurements with no prospective motion correction (a,d), volume-to-volume-based prospective motion correction (b,e) and multislice-to-volume-based prospective motion correction (c,f). In all measurements, a slice-acceleration factor of three was used and the diagram shows the same underlying data without (left) and with (right) retrospective motion correction.

frequency of $\geq$0.68 Hz to properly characterize the respiratory cycle. With a temporal resolution of ~3.33 Hz of the multislice-to-volume-based prospective motion correction, this was easily achieved. The two other graphs in the figure show how the pattern of respiratory motion is closely matched by plots of accumulated motion estimates derived from multislice-to-volume-based prospective motion correction with enabled Kalman filter. The two directions of the measurement which were influenced the most by respiratory motion events are chosen for display.

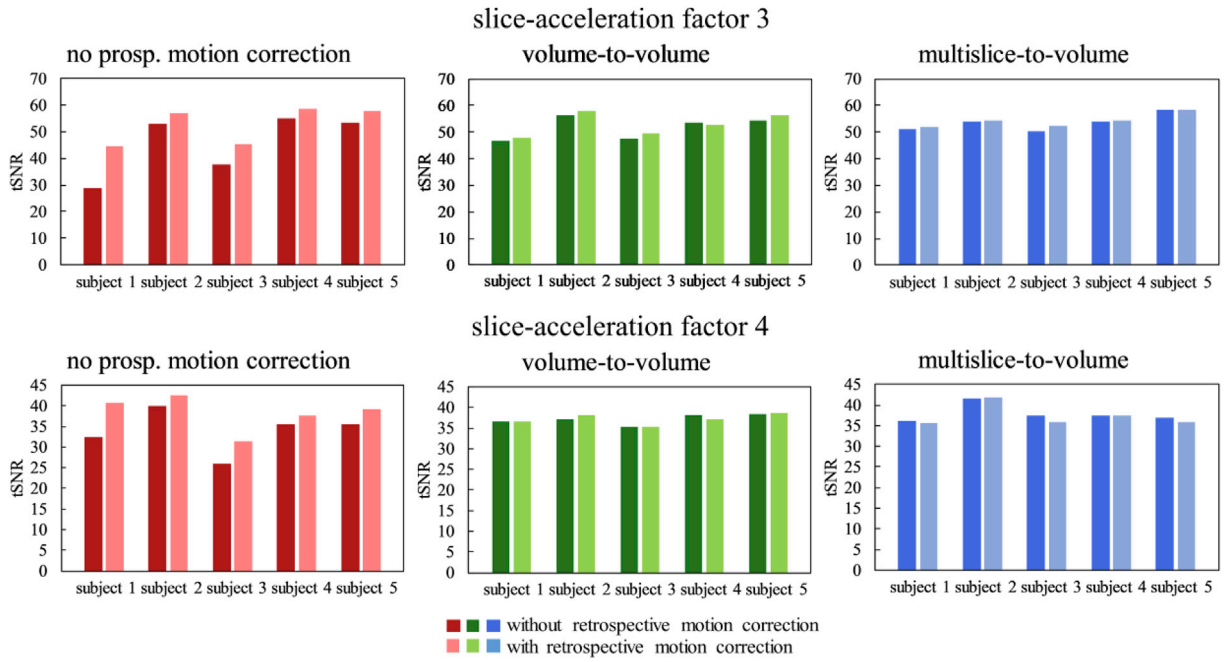

Fig. 9. Temporal SNR values of data acquired using no prospective motion correction (red), volume-to-volume-based prospective motion correction (green) and the proposed multislice-to-volume-based prospective motion correction (blue). The diagram also shows tSNR values after additional retrospective motion correction using SPM12 (light red, light green, light blue). Temporal SNR was only calculated on voxels belonging to the foreground of the image.

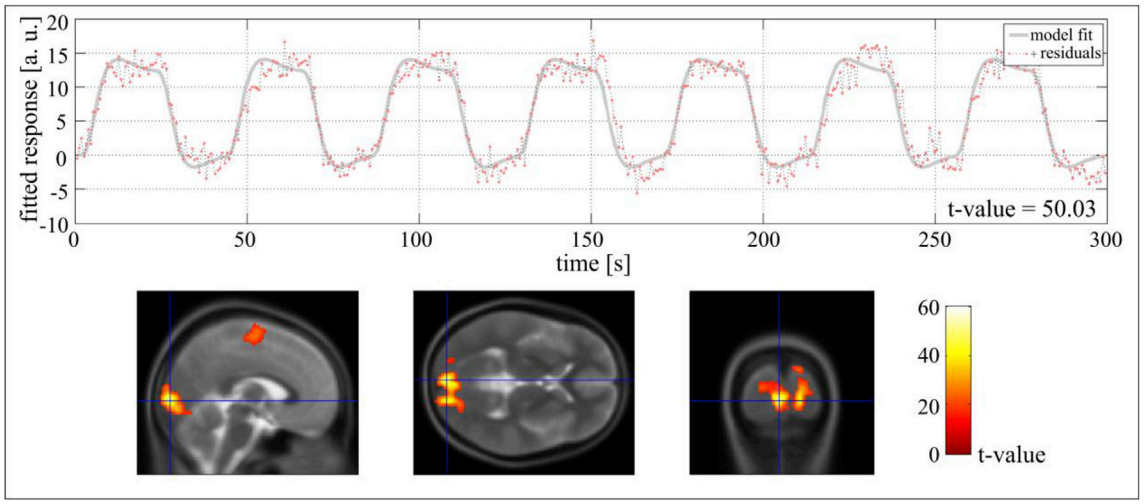

Fig. 10. BOLD response for a measurement with multislice-to-volume-based prospective motion correction, determined by SPM12. The response curve for an individual voxel (top) is shown for the area of highest activation in the visual cortex of the brain activation map, which displays a colormap of t-values resulting from the fMRI analysis (bottom).

The temporal resolution of the volume-to-volume-based prospective motion correction throughout this work was ~0.45 Hz in the first one-subject experiment and ~0.56 Hz (slice-acceleration factor three) and ~0.75 Hz (slice-acceleration factor four) in the five-subject experiment. Only in one of these cases, the Nyquist-Shannon theorem would have been fulfilled to allow the detection of the true respiratory motion. This was mainly driven by skipping one TR to apply the current motion parameters which was necessary in our experiments due to the low inter-volume pause in the sequence, caused by the low TR, together with the necessary calculation times of image registration and slice separation. This effect could be mitigated when using other scan parameters allowing timely feedback execution between the acquisition of two image volumes. Note, however, that with volume-to-volume image registration, the respiratory motion is additionally smoothed out over a whole imaging volume which might not result in the detection of the true respiratory phase.

5. Discussion

The objective of this study has been to identify a high temporal resolution, image-based prospective motion correction technique for simultaneous multislice functional MRI measurements. One experiment was performed in silico to evaluate the accuracy of the image registration and three experiments were performed in vivo for evaluation and comparison with a conventional prospective motion correction technique. Some aspects of these experiments are discussed below.

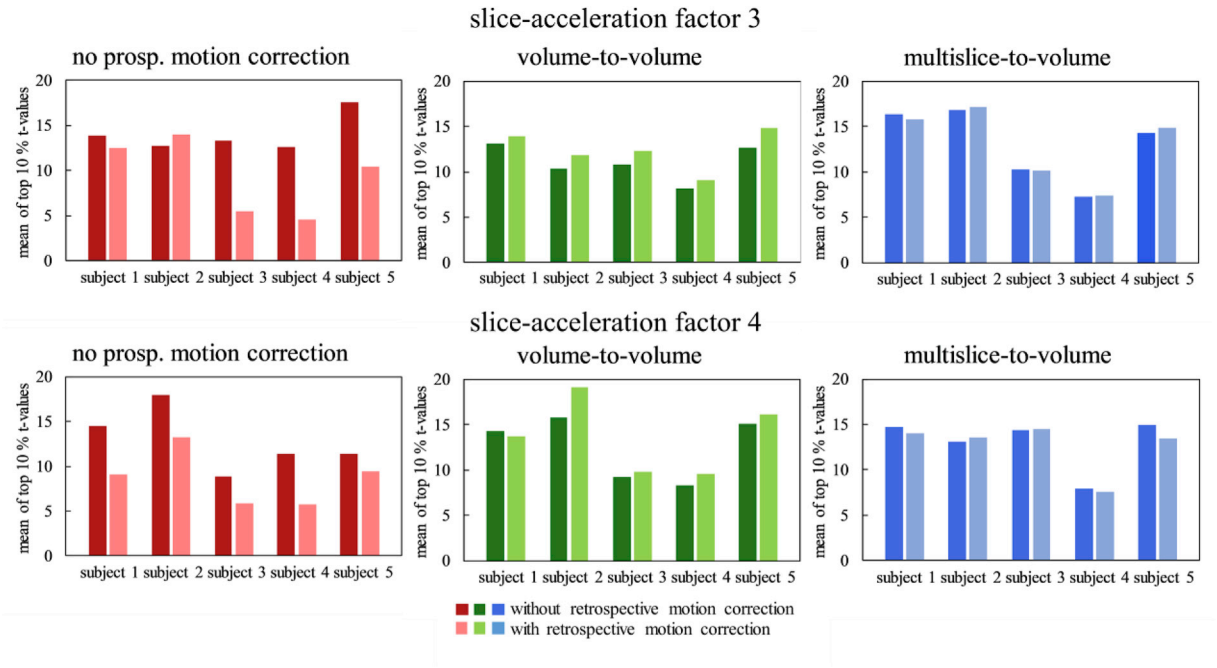

Fig. 11. Brain activation results in terms of the mean of the top 10% of t-values of data acquired using no prospective motion correction (red), volume-to-volume-based prospective motion correction (green) and the proposed multislice-to-volume-based prospective motion correction (blue). The diagram shows results without (dark colors) and with (light colors) additional retrospective motion correction using SPM12.

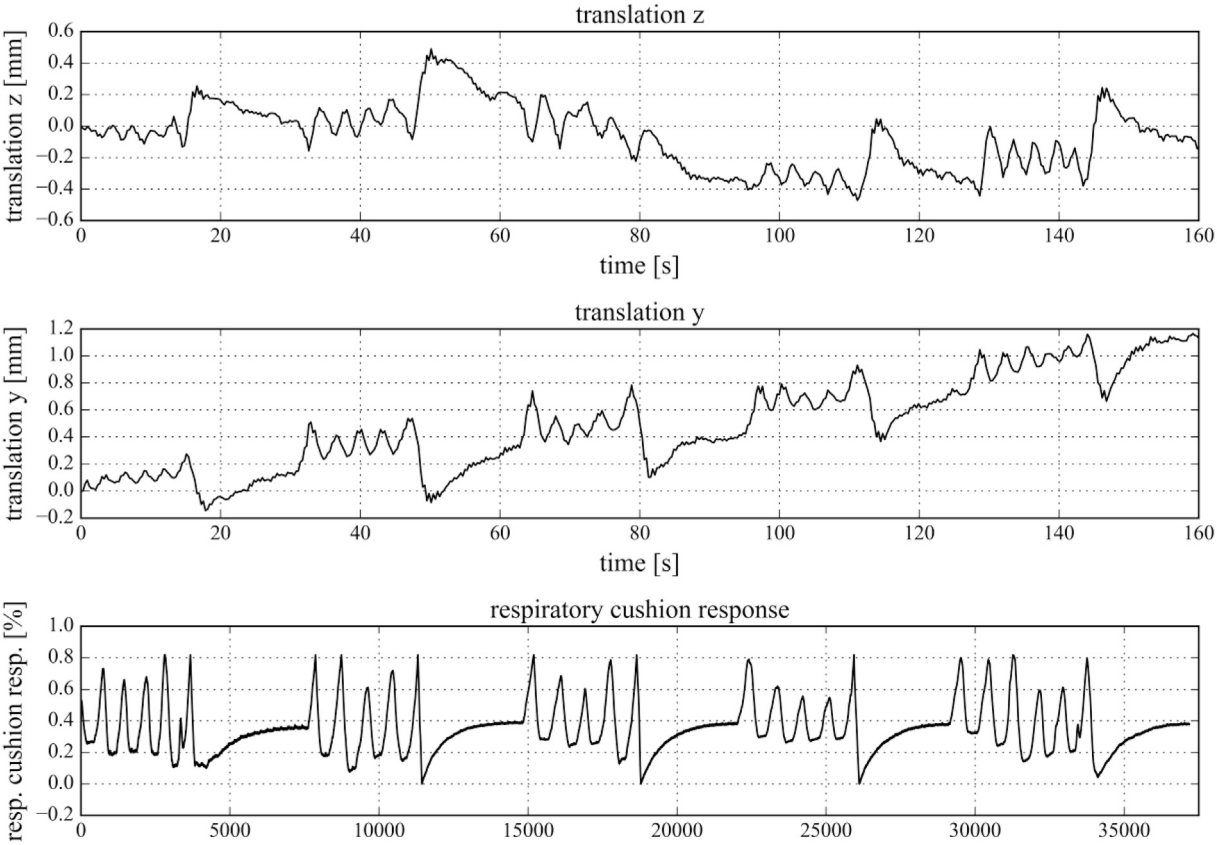

Fig. 12. Motion parameters from a measurement with multiple breathhold events. The two top diagrams show the two directions of the measurement which were influenced the most by respiratory motion events and plot the accumulated motion estimates, acquired during prospective motion correction using multislice-to-volume image registration. The subject performed multiple alternations of 22 s breathholds with interleaved phases of 22 s normal respiration. The prospective motion detection had a temporal resolution of ~3.33 Hz. The graph in the bottom diagram shows the data from the respiratory cushion, synchronized to the motion correction curves. It shows that the respiratory motion was successfully detected by the prospective motion correction when comparing the motion estimates to the respiratory cushion data.

5.1. Random head motion to simulate motion effects

The amount of voluntary subject motion in the first experiment acquired in vivo is shown in the curves without prospective motion correction of Fig. 3. The subject performed head movements within a small range, restricted by the earmuffs and the head coil, leading to motion parameter estimates of up to ±2 mm and ±2°. These were calculated by volume-to-volume-based retrospective motion correction, such that the true underlying motion might be underestimated since the motion state was calculated for a whole TR. Indeed, severe banding artifacts were seen in the data, suggesting a high level of intra-volume motion. This intentional motion performed by the subject may not be a perfect model for real measurements with uncooperative subjects, but it provides a good indication for the performance of the multislice-to-volume-based prospective motion correction technique with this group of subjects. All subsequent measurements did not include intentional head motion of the subjects. However, measurements without intentional head motion showed that the fMRI tasks themselves as well as other factors like discomfort and subsidence of the pillow lead to unintended subject head motion.

5.2. Residual motion parameters and Kalman filtering

The calculation of residual motion parameters for the first experiment acquired in vivo showed the advantage of the higher resolution of the multislice-to-volume-based approach, such that it can adapt to the subject motion faster, resulting in less residual motion. Without additional Kalman filtering, this is only true for strong subject motion where the extent of motion is larger than the outliers in the image detection estimates (see Fig. 3). These outliers can be observed when measuring without intentional head motion, as seen in Fig. 4. They might be caused by imprecision in the image registration procedure due to the reduced amount of image information which is used in the multislice-to-volume method. In the volume-to-volume case, if there are single corrupted slices, the rest of the volume can compensate for this in the registration process and still generate robust motion estimates. In multislice-to-volume image registration, single artifacts or distortions in the images have much more impact on the motion estimates, which is even more problematic when the subset of slices includes one of the topmost slices where the subject only covers a small part of the FOV. This is why multislice-to-volume image registration uses a computationally more intense cost function to extract robust motion estimates from the small number of slices used. In particular, this reduces the effect of localized image distortions, which can be more problematic than when volume-to-volume registration is performed with a large number of slices. Since only a small subset of slices is included in the image registration process, the processing time of the cost function remains low.

A suggested solution to this observation was the addition of a real-time Kalman filter to stabilize the motion estimates used for the prospective motion correction. Fig. 5 shows that the residual motion parameter estimates, retrospectively determined by SPM12, were stable when measuring with the additional real-time Kalman filter, which is why it was used in all subsequent measurements of this work that were performed with multislice-to-volume-based prospective motion correction. Note that the Kalman filter introduces a short delay in the motion correction updates since the system adapts to new motion states more slowly. This is necessary to successfully reduce the incidence of outliers in the motion estimates. In the experimental data, this delay can be observed to be in the range of a single correction step size when sudden, fast motion events occur.

Figs. 6 and 7 summarize the motion estimates of the five-subject experiment. The data indicate that the Kalman filter adds a lot of stability to the motion estimates, resulting in low residual motion. The mean voxel displacements of measurements corrected with volume-to-volume-based prospective motion correction are almost halved when measuring with the suggested multislice-to-volume-based technique. This applies to all subjects and slice-acceleration factors and is not related to the amount of underlying subject motion. An alternative to the Kalman filter would be to use the slices of multiple excitations for image registration, e.g. measuring with slice-acceleration factor three, but waiting for six slices for image registration and with that stabilizing the image registration estimates. These possibilities have to be examined in future work.

The low level of residual motion leads to higher image quality during the scan, shown by the comparison of temporal SNR values without additional retrospective motion correction in Figs. 8 and 9. The results, however, also show the ability of retrospective motion correction to recover image quality during post-processing, shown by the comparable tSNR results after addition of retrospective motion correction which would be used in most fMRI applications. Under the experimental conditions used in this study, the proposed method provided a prospective performance that was comparable to that of the retrospective method, but no clear benefit was observed that could be related to the improved temporal resolution of the new method. However, it is possible that such a benefit will be observed when there is a substantial amount of intra-volume motion and this could be investigated explicitly in future work. The results of temporal SNR analysis also show that image quality degrades when using higher slice-acceleration factors. This is a typical observation when using SMS acquisitions, where an increase in the slice-acceleration factor is linked to a reduction in SNR due to g-factor effects (Breuer et al., 2009; Setsompop et al., 2012). The reduction in image quality could reduce the accuracy of the image registration process. However, the additional slices also add more information to the registration process. We did not further validate the accuracy of the split slice-GRAPPA slice separation in our experiments. Since the auto-calibration data is only acquired at the start of the measurement, motion-induced shifts in slice position between auto-calibration data and imaging scan as well as a change in the loading of the coils can cause ghosting due to false image separation. Visual inspection of the image data showed no severe, subject-position-dependent ghosting artifacts.

A typical challenge when performing evaluation studies on different prospective motion correction techniques is that the subject motion cannot be assumed to be the same for repeated measurements. This was accepted during the study as there is little chance to control the motion without using defined motion protocols. The goal was to evaluate the proposed technique under normal conditions to evoke the amount of subject motion typically seen during fMRI measurements. However, to explore the more extreme case, the level of motion was exaggerated by performing studies without head fixation. Experimental bias between techniques was minimized by varying the order of measurements between subjects and by repositioning the subjects between measurement blocks.

5.3. Temporal resolution of motion correction updates and hardware limits

In this study, the suggested prospective motion correction technique enabled a temporal resolution of motion correction updates of below 300 ms when measuring with the specified imaging protocols. This is a large improvement when compared to conventional volume-to-volume-based prospective motion correction and, as shown in Fig. 12, also allows for adequate reconstruction of respiratory motion. The calculation of GRAPPA weights from the auto-calibration data required a waiting time in the sequence until the calculation is done. In the experiments, the calculation time of the GRAPPA weight set was about 10 s for a slice-acceleration factor of three and 13 s for a slice-acceleration factor of four. However, this time could also be used to perform dummy scans to establish steady-state magnetization prior to the first imaging scan. These calculation times are, besides the imaging protocol, mainly dependent on the computational performance of the scanner hardware. Theoretically, multislice-to-volume-based prospective motion correction allows for motion correction updates after each RF excitation and EPI readout, since the amount of data is sufficient to calculate motion estimates. However, image reconstruction, SMS image separation and image registration

require a finite amount of computation time before the updates are available. This time was substantially reduced in this study by using all available processor threads provided by the scanner hardware. However, since the calculation time of these algorithms strongly scales with the multi-threading factor, the processing time can be further reduced with more powerful scanner hardware than the seven-year-old scanner used in the experiments; this would include processors with more cores or the use of graphic cards. Considering software optimization, there is some room for improvement in the use of multi-threading for the image registration calculation. A specific and more efficiently multi-threaded implementation of the registration method could already help in reducing some of the calculation time. Also, some registration parameters could be optimized without a significant loss of accuracy. For this proof-of-concept study, however, we chose these parameters conservatively to ensure optimal registration performance.

5.4. Functional MRI study results

The fMRI study results from the five subjects show high variation in brain activity between subjects and measurements as expected in these studies, especially considering the small study size. This makes it particularly difficult to draw conclusions from the data. The results in Fig. 11 compare the mean of the top 10% of t-values of the same measurement when analyzing with and without retrospective motion correction. Uncorrected head motion which correlates with the fMRI paradigm can lead to false activation and increase the determined t-values as seen in the results of measurements without prospective motion correction. On the other hand, the brain activation estimates originating from the volume-to-volume-based prospective motion correction can be further increased by using retrospective motion correction, also indicating residual motion in the data. The results of measurements using the proposed prospective motion correction technique show a high consistency between mean t-values before and after applying retrospective motion correction. As there is no gold standard in the comparison between these methods, some caution needs to be exercised when interpreting the results. The data do not demonstrate that the proposed multislice-to-volume method provides fMRI results with the highest accuracy, or indeed with the least motion sensitivity, but the highly consistent t-statistics with and without retrospective motion correction suggests a robust performance. However, this does not necessarily mean that the proposed technique can obtain motion-insensitive fMRI measurements. It suggests that most image misalignments which occurred during the measurement were successfully corrected by the prospective motion correction procedure, but it does not establish whether or not the fMRI results from the motion-corrected data are confounded by the motion. Further examination is required for a detailed investigation to determine the effect of multislice-to-volume-based prospective motion correction on the fMRI statistics in real fMRI experiments. Additional validation studies should also be performed with uncooperative subjects where the improvements due to prospective motion correction are likely to be more substantial. It would also be of interest to validate the method with simultaneous optical tracking as a reference.

5.5. Comparison with other prospective motion correction techniques

The volume-to-volume-based prospective motion correction has been well accepted in neuroscience imaging, but became impractical on current MRI systems with the introduction of SMS imaging due to the requirement for real-time slice separation. The proposed technique presents a solution that can practically be used on the scanner and combines the advantages of both SMS imaging and prospective motion correction with high temporal resolution. In the experiments, multislice-to-volume-based prospective motion correction showed higher motion correction capabilities when compared to the conventional volume-to-volume-based approach. There is no obvious disadvantage in using the proposed technique, but it can significantly increase the temporal resolution of motion correction updates without a substantial penalty in the accuracy of parameter estimates. This enables the possibility of sub-TR prospective motion correction and might also increase the volume integrity of single image volumes. Multislice-to-volume-based prospective motion correction can be used with a range of slice-acceleration factors to adjust the accuracy of image registration and the temporal resolution. It can also be used for fMRI without slice acceleration, in which the method would wait for a certain number of slices before starting the image registration process. However, this would require an adapted slice-ordering scheme, similar to that shown in Hoinkiss and Porter (2017). Prospective motion correction using external hardware, on the other hand, can be used with almost any pulse sequence and imaging protocol without a change in motion correction accuracy. The comparison to these techniques was not made in this study, but previous work shows that they can provide a higher temporal resolution than the values achieved in this study. However, as discussed above, the speed of the proposed motion correction technique could be further increased with more powerful scanner hardware. Since the measurements were performed on a seven-year-old MRI scanner, adapting the proposed technique to more recent scanner hardware would already help to increase the temporal resolution of motion correction updates. This would provide a performance closer to that of camera-based prospective motion correction without the need for external hardware. Apart from the financial benefits of avoiding the installation of additional hardware, the image-based approach has the advantage of avoiding external markers and bite bars, which would limit application in routine clinical studies.

6. Conclusion

In this study, prospective motion correction using multislice-to-volume image registration was combined with the simultaneous acquisition of multiple slices. Its application to slice-accelerated functional MRI was described and evaluated. Due to the simultaneous excitation of multiple slices, only a single RF excitation is required to get sufficient image data for motion correction. This offers a high temporal resolution and the possibility of intra-volume motion correction. Study results show a substantial reduction for in-plane and out-of-plane motion parameters when compared to conventional volume-to-volume-based prospective motion correction both in measurements with and without intentional head movements. An analysis of temporal signal-to-noise ratio as well as brain activation results shows high consistency between the results before and after additional retrospective motion correction when using the proposed technique, indicating successful prospective motion correction.

Role of the funding source

This work was supported by the FhG Internal Programs under Grant No. Attract 142-600172.

Declaration of interest

The authors Daniel Christopher Hoinkiss and David Andrew Porter applied for a patent which, if accepted, will be valid in various countries. The method mentioned in the submitted manuscript is part of this patent.

Data and code availability statement

Due to proprietary regulations of the scanner manufacturer, the source code of the imaging sequence, image reconstruction and prospective motion correction cannot be made available to the public. Image data and source code for data analysis will be provided on request by the corresponding author.

Acknowledgements

The authors are grateful to Robert Frost and the Welcome Centre For Integrative Neuroimaging at Oxford University for providing source code for their slice-GRAPPA implementation and to Klaus Eickel from Fraunhofer MEVIS for valuable discussion and support.

References

Aksoy, M., et al., 2011. Real-time optical motion correction for diffusion tensor imaging. Magn. Reson. Med. 66, 366–378. https://doi.org/10.1002/mrm.22787.

Andersson, J.L.R., et al., 2018. Susceptibility-induced distortion that varies due to motion: correction in diffusion MR without acquiring additional data. Neuroimage 171, 277–295. https://doi.org/10.1016/j.neuroimage.2017.12.040.

Bandettini, P.A., et al., 1992. Time course EPI of human brain function during task activation. Magn. Reson. Imag. 25, 390–397. https://doi.org/10.1002/mrm.1910250220.

Beall, E.B., Lowe, M.J., 2014. SimPACE: generating simulated motion corrupted BOLD data with synthetic-navigated acquisition for the development and evaluation of SLOMOCO: a new, highly effective slicewise motion correction. Neuroimage 101, 21–34. https://doi.org/10.1016/j.neuroimage.2014.06.038.

Benner, T., Kouwe, A.J.W., Kirsch, J.E., Sorensen, A.G., 2006. Real-time RF pulse adjustment for B0 drift correction. Magn. Reson. Med. 56, 204–209. https://doi.org/10.1002/mrm.20936.

Bettinardi, V., et al., 1991. Head holder for PET, CT, and MR studies. J. Comput. Assist. Tomogr. 15, 886–892. https://doi.org/10.1097/00004728-199109000-00034.

Breuer, F.A., et al., 2005. Controlled aliasing in parallel imaging results in higher acceleration (CAIPIRINHA) for multi-slice imaging. Magn. Reson. Med. 53, 684–691. https://doi.org/10.1002/mrm.20401.

Breuer, F.A., et al., 2009. General formulation for quantitative G-factor calculation in GRAPPA reconstructions. Magn. Reson. Med. 62, 739–746. https://doi.org/10.1002/mrm.22066.

Cauley, S.F., et al., 2014. Interslice leakage artifact reduction technique for simultaneous multislice acquisitions. Magn. Reson. Med. 72, 93–102. https://doi.org/10.1002/mrm.24898.

Chen, L., et al., 2015. Evaluation of highly accelerated simultaneous multi-slice EPI for fMRI. Neuroimage 104, 452–459. https://doi.org/10.1016/j.neuroimage.2014.10.027.

Cheng, H., Puce, A., 2014. Reducing respiratory effect in motion correction for EPI images with sequential slice acquisition order. J. Neurosci. Methods 227, 83–89. https://doi.org/10.1016/j.jneumeth.2014.02.007.

Cox, R.W., 1996. AFNI: software for analysis and visualization of functional magnetic resonance neuroimages. Comput. Biomed. Res. 29, 162–173. https://doi.org/10.1006/cbmr.1996.0014.

Edward, V., et al., 2000. Quantification of fMRI artifact reduction by a Novel plaster cast head holder. Hum. Brain Mapp. 11, 207–213. https://doi.org/10.1002/1097-0193(200011)11:3<207::AID-HBM60>3.0.CO;2-J.

Feinberg, D.A., Setsompop, K., 2013. Ultra-fast MRI of the human brain with simultaneous multi-slice imaging. J. Magn. Reson. 229, 90–100. https://doi.org/10.1016/j.jmr.2013.02.002.

Friston, K.J., et al., 2007. Statistical Parametric Mapping: the Analysis of Functional Brain Images. Academic Press. https://doi.org/10.1016/B978-0-12-372560-8.X5000-1 s.l.

Haacke, E.M., Patrick, J.L., 1986. Reducing motion artifacts in two-dimensional fourier transform imaging. Magn. Reson. Imag. 4, 359–376. https://doi.org/10.1016/0730-725X(86)91046-5.

Hoinkiss, D.C., Porter, D.A., 2017. Prospective motion correction in 2D multishot MRI using EPI navigators and multislice-to-volume image registration. Magn. Reson. Med. 78, 2127–2135. https://doi.org/10.1002/mrm.26951.

Hoinkiss, D.C., et al., 2018. Prospective motion correction in multiband fMRI using multislice-to-volume image registration. In: Proceedings of the Joint Annual Meeting of the International Society for Magnetic Resonance in Medicine and the European Society of Magnetic Resonance in Medicine and Biology, p. 1170. Paris, France.

Huang, L.-K., Wang, M.-J.J., 1995. Image thresholding by minimizing the measures of fuzziness. Pattern Recogn. 28, 41–51. https://doi.org/10.1016/0031-3203(94)E0043-K.

Huang, P., et al., 2018. Prospective motion correction improves the sensitivity of fMRI pattern decoding. Hum. Brain Mapp. 39 (10), 4018–4031. https://doi.org/10.1002/hbm.24228.

Jenkinson, M., Bannister, P., Brady, M., Smith, S., 2002. Improved optimization for the robust and accurate linear registration and motion correction of brain images. Neuroimage 17, 825–841. https://doi.org/10.1006/nimg.2002.1132.

Kalman, R.E., 1960. A new approach to linear filtering and prediction problems. Trans. ASME J. Basic Eng. 82 (D), 35–45. https://doi.org/10.1115/1.3662552.

Kwong, K.K., et al., 1992. Dynamic magnetic resonance imaging of human brain activity during primary sensory stimulation. Proc. Natl. Acad. Sci. U.S.A. 89, 5675–5679.

Larkman, D.J., et al., 2001. Use of multicoil arrays for separation of signal from multiple slices simultaneously excited. J. Magn. Reson. Imaging 13, 313–317. https://doi.org/10.1002/1522-2586(200102)13:2<313::AID-JMRI1045>3.0.CO;2-W.

Maclaren, J., Speck, O., Hennig, J., Zaitsev, M., 2009. A Kalman filtering framework for prospective motion correction. In: Proceedings of the 17th Annual Meeting of the International Society for Magnetic Resonance in Medicine, p. 4602. Honolulu, HI, United States.

Maclaren, J., Herbst, M., Speck, O., Zaitsev, M., 2013. Prospective motion correction in brain imaging: a review. Magn. Reson. Med. 69 (3), 621–636. https://doi.org/10.1002/mrm.24314.

Mansfield, P., 1977. Multi-planar image formation using NMR spin echoes. J. Phys. C Solid State Phys. 10, L55–L58. https://doi.org/10.1088/0022-3719/10/3/004.

Mattes, D., et al., 2001. Nonrigid multimodality image registration. In: Proceedings of SPIE - the International Society for Optical Engineering, pp. 1609–1620. San Diego, CA, United States.

Mattes, D., et al., 2003. PET-CT image registration in the chest using free-form deformations. IEEE Trans. Med. Imaging 22, 120–128. https://doi.org/10.1109/TMI.2003.809072.

Nunes, R.G., Hajnal, J.V., Golay, X., Larkman, D.J., 2006. Simultaneous slice excitation and reconstruction for singleshot EPI. In: Proceedings of the 14th Annual Meeting of the International Society for Magnetic Resonance in Medicine, p. 293. Seattle, WA, United States.

Preibisch, C., Castrillon, J.G., Buehrer, M., Riedl, V., 2015. Evaluation of multiband EPI acquisitions for resting state fMRI. PLoS One 10. https://doi.org/10.1371/journal.pone.0136961.

Setsompop, K., et al., 2012. Blipped-controlled aliasing in parallel imaging for simultaneous multislice echo planar imaging with reduced g-factor penalty. Magn. Reson. Med. 67, 1210–1224. https://doi.org/10.1002/mrm.23097.

Teruel, J.R., Kuperman, J.M., Dale, A.M., White, N.S., 2018. High temporal resolution motion estimation using a self-navigated simultaneous multi-slice echo planar imaging acquisition. J. Magn. Reson. Imaging 48, 780–787. https://doi.org/10.1002/jmri.25953.

Thesen, S., Heid, O., Mueller, E., Schad, L.R., 2000. Prospective acquisition correction for head motion with image-based tracking for real-time fMRI. Magn. Reson. Med. 44, 457–465. https://doi.org/10.1002/1522-2594(200009)44:3<457::AID-MRM17>3.0.CO;2-R.

Thesen, S., Krüger, G., Müller, E., 2003. Absolute correction of B0 fluctuations in echo-planar imaging. In: Proceedings of the 11th Annual Meeting of the International Society for Magnetic Resonance in Medicine. Canada, Toronto, p. 1025.

Thulborn, K.R., Waterton, J.C., Matthews, P.M., Radda, G.K., 1982. Oxygenation dependence of the transverse relaxation time of water protons in whole blood at high field. Biochim. Biophys. Acta 714, 265–270. https://doi.org/10.1016/0304-4165(82)90333-6.

Wansapura, J.P., Holland, S.K., Dunn, R.S., Ball, W.S., 1999. NMR relaxation times in the HumanBrain at 3.0 tesla. J. Magn. Reson. Med. 9, 531–538. https://doi.org/10.1002/(SICI)1522-2586(199904)9:4<531::AID-JMRI4>3.0.CO;2-L.

White, N., et al., 2010. PROMO: real-time prospective motion correction in MRI using image-based tracking. Magn. Reson. Med. 63, 91–105. https://doi.org/10.1002/mrm.22176.

Yoo, T.S., , et al.Westwood, J., 2002. Medicine meets virtual reality. IOS Press, Amsterdam, pp. 586–592 s.l.

Zaitsev, M., et al., 2006. Magnetic resonance imaging of freely moving objects: prospective real-time motion correction using an external optical motion tracking system. Neuroimage 31, 1038–1050. https://doi.org/10.1016/j.neuroimage.2006.01.039.

Zaitsev, M., Akin, B., LeVan, P., Knowles, B.R., 2017. Prospective motion correction in functional MRI. Neuroimage 154, 33–42. https://doi.org/10.1016/j.neuroimage.2016.11.014.